Acta Oceanol. Sin., 2017, Vol. 36, No. 3, P. 52–59
DOI: 10.1007/s13131-017-1040-0
http://www.hyxb.org.cn
E-mail: hyxbe@263.net

Comparison of TMI and AMSR-E sea surface temperatures with Argo near-surface temperatures over the global oceans

CHEN Xingrong[1], LIU Zenghong[2, 3]*, SUN Chaohui[3], WANG Haiyan[1]

[1] National Marine Environmental Forecasting Center, State Oceanic Administration, Beijing 100081, China

[2] State Key Laboratory of Satellite Ocean Environment Dynamics, Second Institute of Oceanography, State Oceanic Administration, Hangzhou 310012, China

[3] Second Institute of Oceanography, State Oceanic Administration, Hangzhou 310012, China

Received 26 February 2016; accepted 25 April 2016

Abstract

Satellite-derived sea surface temperatures (SSTs) from the tropical rainfall measuring mission (TRMM) microwave imager (TMI) and the advanced microwave scanning radiometer for the earth observing system (AMSR-E) were compared with non-pumped near-surface temperatures (NSTs) obtained from Argo profiling floats over the global oceans. Factors that might cause temperature differences were examined, including wind speed, columnar water vapor, liquid cloud water, and geographic location. The results show that both TMI and AMSR-E SSTs are highly correlated with the Argo NSTs; however, at low wind speeds, they are on average warmer than the Argo NSTs. The TMI performs slightly better than the AMSR-E at low wind speeds, whereas the TMI SST retrievals might be poorly calibrated at high wind speeds. The temperature differences indicate a warm bias of the TMI/AMSR-E when columnar water vapor is low, which can indicate that neither TMI nor AMSR-E SSTs are well calibrated at high latitudes. The SST in the Kuroshio Extension region has higher variability than in the Kuroshio region. The variability of the temperature difference between the satellite-retrieved SSTs and the Argo NSTs is lower in the Kuroshio Extension during spring. At low wind speeds, neither TMI nor AMSR-E SSTs are well calibrated, although the TMI performs better than the AMSR-E.

Key words: Argo, near-surface temperature, tropical rainfall measuring mission (TRMM) microwave imager, advanced microwave scanning radiometer for the earth observing system, sea surface temperature

Citation: Chen Xingrong, Liu Zenghong, Sun Chaohui, Wang Haiyan. 2017. Comparison of TMI and AMSR-E sea surface temperatures with Argo near-surface temperatures over the global oceans. Acta Oceanologica Sinica, 36(3): 52–59, doi: 10.1007/s13131-017-1040-0

1 Introduction

The world's oceans cover approximately 70% of the earth's surface and absorb 70% of incoming solar radiation. The spatial variation in the heat content of the oceans has considerable influence on atmospheric motion that leads to regional- and global-scale climate changes. Sea surface temperature (SST) is an important physical parameter that affects the exchange of heat, momentum, and water vapor between the atmosphere and the ocean, which is very important in determining air-sea interaction and climate change (Curry et al., 2004). SST data have been used for research in many fields such as weather forecasting, climate prediction, ocean circulation, ocean fisheries, and the oceanic ecological environment (Suarez and Schopf, 1988; McPhaden, 1999). There are two primary methods for measuring the SST: *in situ* observation and satellite remote sensing. Traditional *in situ* SST observations, obtained mainly from gauging stations, ships, and moored and drifting buoys, have high accuracy at depths of 0.01–7.00 m but with relatively poor spatiotemporal resolution and continuity. Compared with *in situ* observations, satellite remote sensing has much higher spatiotemporal coverage. Although the obtained sea "skin" temperature might not be representative of the "bulk" temperature, the advantages offered by satellites make them indispensable for SST measurements (Barton, 1995; Donlon et al., 2002, 2007).

SST observations can be derived from both infrared and microwave radiometers that are carried on a number of satellites. Infrared sensing, such as AVHRR and MODIS, is able to acquire high-resolution SSTs at 1 km spatial resolution but it is susceptible to the effects of the atmospheric environment. Thus, it might not provide valid data in cases of cloud or high columnar water vapor content. Its biases are mainly due to diurnal variability, water vapor attenuation, presence of atmospheric aerosols, and incomplete removal of cloud contamination (Brown et al., 1985; McClain, 1989; Emery at al., 1994). The regional analyses of the SST indicate that diurnal SST warming can exceed 6°C and that the magnitude of this warming depends on both solar insolation and wind speed (Flament et al., 1994; Gentemann et al., 2003, 2008; Gentemann and Minnett, 2008; Merchant et al., 2008). Microwave sensing is able to measure the SST in all weathers and all of the time because the operational wavelength is longer than the scales of water vapor and aerosols (Wentz, 1998; Wentz et al., 2000). Therefore, a microwave technology has been applied increasingly to the SST measurement, e.g., the tropical rainfall measuring mission (TRMM) microwave imager (TMI), and Aqua

Foundation item: The National Basic Research Program (973 Program) of China under contract No. 2013CB430301; the National Natural Science Foundation of China under contract Nos 41440039, 41206022 and 41406022; the Public Science and Technology Research Funds Projects of Ocean under contract No. 201305032.

*Corresponding author, E-mail: liuzenghong@139.com

and ADEOS-2 onboard the advanced microwave scanning radiometer for the earth observing system (AMSR-E). However, the longer wavelength leads to lower spatial resolution (≈50 km) and to greater sensitivity to the effects of sea surface wind and waves, as well as to inland interference signals (Guan and Kawamura, 2003).

To overcome the uncertainty in satellite-retrieved SSTs, *in situ* observations are needed for corroborative evaluation. To validate satellite-retrieved SSTs, buoy-measured SSTs and expendable bathythermographs (XBTs) that measure the subsurface (1–5 m) "bulk" SST have been widely adopted (Pandey and Kniffen, 1991; Bhat et al., 2004; Gentemann et al., 2004; Muraleedharan et al., 2004; Parekh et al., 2007). Given the growth of the global Argo array, these have become a major source of subsurface oceanic data. Bhaskar et al. (2009) compared the AMSR-E and the TMI SSTs with the Argo-derived nominal surface temperatures over the Indian Ocean and found good spatial correlation between the Argo- and satellite-retrieved SSTs. The Argo nominal SST used by Bhaskar et al. (2009) is typically measured at a depth of between 3 and 10 m, which might have considerable difference from the skin or subskin SST. To avoid degrading the salinity accuracy by ingesting sea surface contaminants, a conductivity/temperature/depth pump installed on a float is turned off at approximately 5 m beneath the surface as the Argo float ascends. To meet the need of acquiring near-surface temperatures (hereafter, NSTs) for validation of satellite-retrieved SSTs, increasing numbers of floats are designed to sample NSTs without an extra sensor. Thus, they are able to retrieve measurements of 5–15 NSTs at depths of 0–5 m but not measurements of the salinity.

In this study, we compared TMI and AMSR-E SSTs with Argo NSTs, which were obtained from Argo profiling floats over the global oceans, to evaluate the performance of the TMI and AMSR-E retrievals. In addition, a comparison of the TMI and the AMSR-E SSTs with Argo NSTs in the region of the Kuroshio and its extension was performed. The data and the method used in the study are discussed in Section 2. The results and their discussion are presented in Section 3, and the conclusions are given in Section 4.

2 Data and method

2.1 *TMI and AMSR-E microwave SSTs*

The SSTs retrieved by the TMI and the AMSR-E are used widely in oceanic and climatic research. The TMI microwave sensor, launched on November 26, 1997, flies on a non-sun-synchronous orbit and it has a resolution of 6–50 km. The AMSR-E is a passive microwave sensor with a resolution of 5.4–56.0 km that was launched with the Aqua satellite in May 2002 (but failed in October 2011). The Aqua satellite flies on a sun-synchronous orbit that crosses the equator at 13:30 local time (LT) on northward (ascending) passes and at 01:30 on southward (descending) passes. The SST products from the TMI and the AMSR-E have been validated by *in situ* measurements from buoys, high-resolution XBTs, hull-mounted thermosalinographs, and Argo NSTs (Gentemann et al., 2004; Dong et al., 2006; Bhaskar et al., 2009).

The SSTs retrieved by the TMI and the AMSR-E were provided by remote sensing systems, Santa Rose, CA, USA (Wentz, 1998; Wentz and Meissner, 1999). The TMI SSTs are released on a 0.25°×0.25° grid over the global tropics (±39.875°), whereas the AMSR-E SSTs are available globally (±89.875°) with the same spatial resolution. The daily SST product (Version 4) from the TMI and the daily passes of the SST product (Version 7) from the AMSR-E were used in this study. These data sets also included wind speed (measured using the 10.65 and 37.0 GHz channels from the TMI and the 10.7 and 18.7 GHz channels from the AMSR-E), atmospheric water vapor, liquid cloud water, and rainfall rate. The TMI instrument was calibrated carefully using SSM/I collocations based on the methodology described by Wentz et al. (2001). Brightness temperatures were corrected for atmospheric effects using a radiative transfer model (Wentz and Meissner, 1999), whereby the algorithm constants were tuned slightly by intercomparison with *in situ* and climatological observations. The AMSR-E has an onboard calibration system that compensates continuously for variations in the gain and noise temperature of the radiometer. The two vital components of this calibration system are the cold mirror and the hot reference load. Wentz et al. (2003) used coincident measurements from collocated observations from other satellites to develop a system for predicting the temperature of the hot reference. One shortcoming of their procedure is that the *in situ* data available for the calibration of the satellite data were largely concentrated in the tropics.

2.2 *Argo NSTs*

The Argo NST data used in this study were non-pumped temperatures collected by the APEX, PROVOR, and ARVOR profiling floats over the global oceans from October 2008 to March 2012. These floats were deployed and are processed by the British Oceanographic Data Centre, Indian National Centre for Ocean Information Services, Japan Meteorological Agency, Scripps Institution of Oceanography, and University of Washington. Their compiled data are made available on the National Oceanography Centre's (UK) ftp site (ftp://ftp.pol.ac.uk/pub/bodc/argo/NST/). Overall, 409 floats were used in our study, and the uppermost temperature (above 1 m) of each profile was selected for comparison with the satellite-retrieved SSTs.

Each Argo NST was matched to the TMI/AMSR-E measurements collected on the same day, the prior day, and 1 d later. A spatial window of 0.8°×0.5° was chosen to ensure more than one satellite SST retrieval matched a corresponding Argo profile location for each satellite pass. Those selected TMI/AMSR-E observations measured by ascending and descending passes for each day were then interpolated linearly to the Argo measurement point. To minimize diurnal effects, a temporal window of ±5 h was selected for pairing the Argo and TMI/AMSR-E observations. If more than one of the interpolated TMI/AMSR-E retrievals fell into a specific time window, an averaged TMI/AMSR-E observation was computed; otherwise, the nearest SST was selected. After careful assessment of the matchups, abnormal measurements (probably due to transmission errors) from five NST profiles were discarded. Therefore, 3 191 and 3 379 data pairs for the TMI and the AMSR-E, respectively, were matched for this analysis. Figure 1 shows the geographic distribution of the TMI/Argo and AMSR-E/Argo data pairs employed for our analysis. Most TMI/Argo pairs are located (1) near the Kuroshio, Oyashio, and Kuroshio Extension in the northern Pacific, (2) between 15°–40°S in the southern Pacific, (3) in the southern Indian Ocean, especially near Madagascar, and (4) in the southern Atlantic. The AMSR-E/Argo pairs have similar distribution but with many additional data pairs in the Southern Ocean (south of 40°S) and high latitudes (north of 40°N) of the northern Pacific and northern Atlantic.

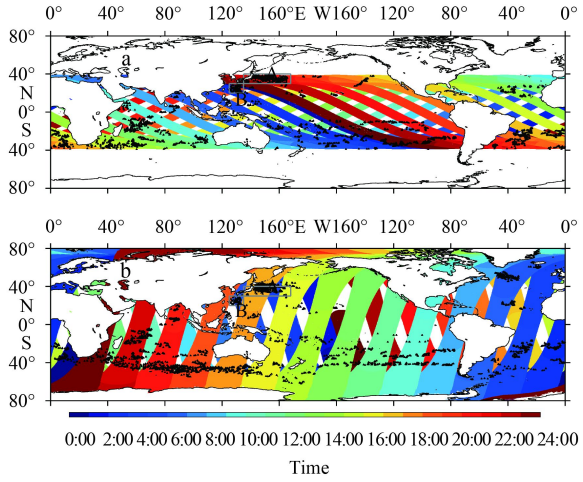

Fig. 1. Match-ups between ascending/descending passes of TMI (a) and AMSR-E (b), and Argo profiles. Both TMI and AMSR-E measurements were observed on January 1, 2010, and their times of passes are indicated by color swaths. The Argo profiles are marked as black triangles. Boxes A (30°–40°N, 135°–168°E) and B (20°–30°N, 125°–135°E), marked by gray rectangles, indicate the Kuroshio and Kuroshio Extension regions.

3 Results and discussion

3.1 *Diurnal variability from Argo temperatures*

To check the diurnal variability in the upper ocean, the near-surface and nominal surface (5 m was selected here) temperatures were selected and compared for each Argo temperature profile. Figure 2 shows the temperature difference between the Argo near-surface and 5 m temperatures, bin-averaged based on the LT. A pronounced diurnal warming can be observed between 10:00 and 19:00 LT, with maximum warming of about 0.1°C occurring at 14:00–15:00 LT. Accompanying the diurnal warming, the variability of the temperature difference increases by 0.33°C with a mean standard deviation of about 0.23°C. A diurnal cooling before 08:00 LT can be seen, with average cooling of about 0.07°C and standard deviation of 0.10°C. On the basis of our analysis, the maximum warming and cooling can be as much as approximately 4.5°C.

A seasonal dependence of the temperature difference exists in both the northern and southern Hemispheres (Fig. 3). The warm bias is most pronounced in the summer months, which is a result of increasing stratification in the upper ocean. This warm bias is more significant in the Southern Hemisphere (about 0.05°C on average) than in the northern Hemisphere. Furthermore, the standard deviation of diurnal warming in the southern Hemisphere (mean value of 0.26°C) is much lower than in the Northern Hemisphere. A cold bias can be observed in the winter months, which is attributable to seasonal changes in upper-ocean stratification. However, the standard deviation of the temperature difference (~0.08°C) is smaller than in the summer months because stronger winter winds reduce the background stratification.

3.2 *Argo NSTs versus TMI/AMSR-E SSTs*

Scatter plots of the TMI and the AMSR-E SSTs and the Argo NSTs are shown in Fig. 4. Overall, the TMI/AMSR-E SSTs and the Argo NSTs show good agreement over the global oceans, with

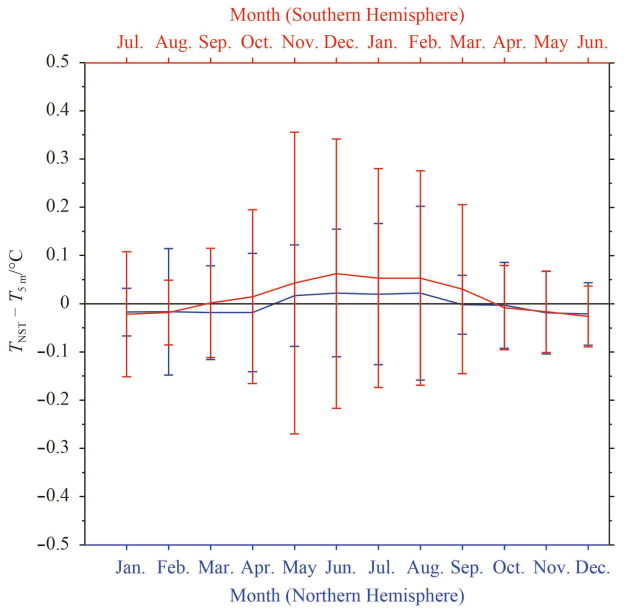

Fig. 3. Argo NSTs minus Argo 5 m temperatures, bin-averaged based on month for the Northern Hemisphere (blue) and the Southern Hemisphere (red). Error bars are twice the standard error for each bin. Here, we adjusted the month so that Month 1 is January for the Northern Hemisphere and July for the Southern Hemisphere.

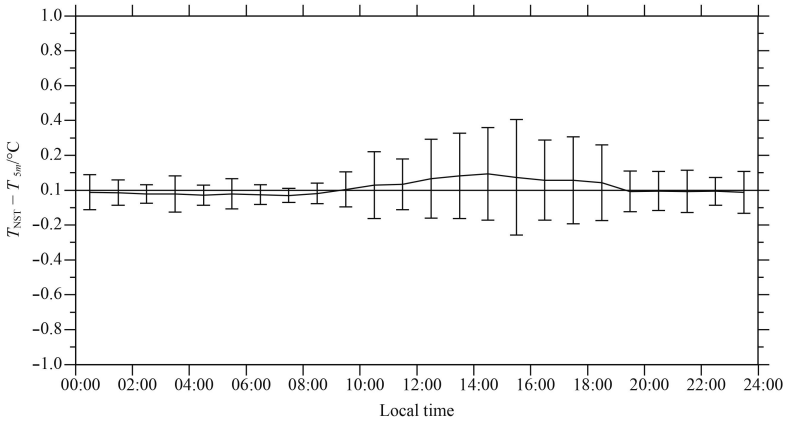

Fig. 2. Argo NSTs minus Argo 5 m temperatures, bin-averaged based on local time. Error bars are twice the standard error for each bin.

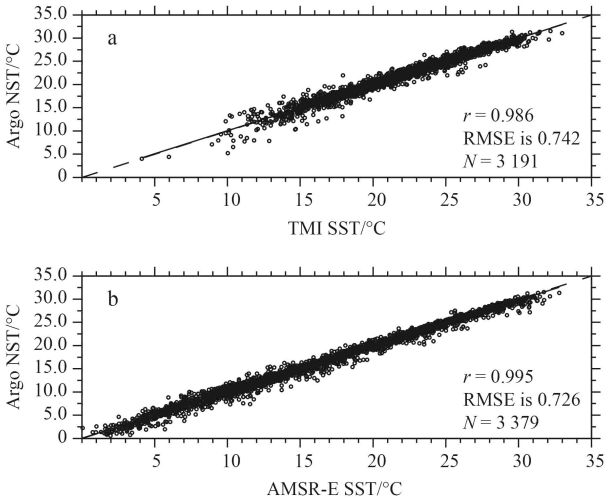

Fig. 4. Scatter plots of Argo NSTs against TMI (a) and AMSR-E SSTs (b) during October 2008 to March 2012. Dashed lines show a linear regression.

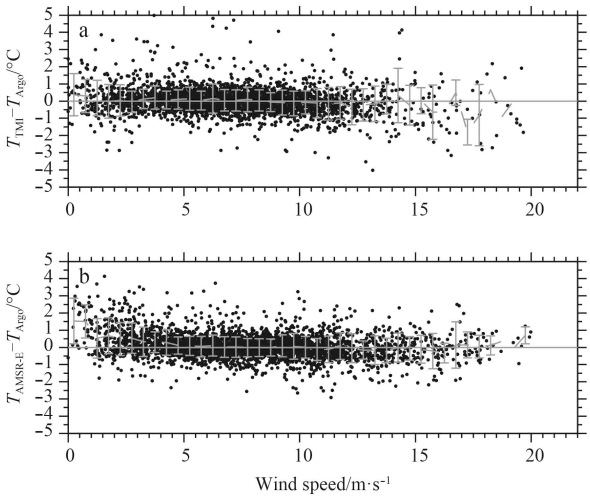

Fig. 5. Scatter plots of TMI (a) and AMSR-E SSTs (b) minus Argo NSTs versus wind speed measured by TMI (measured using the 10.65 GHz channel) and AMSR-E (measured using the 10.7 GHz channel), respectively. Bin-averaged temperature differences based on latitude are marked as gray dashed lines. Error bars are twice the standard error for each bin (standard deviation is not calculated when the number of data pairs is less than 5 in each bin).

correlation coefficients of 0.986 and 0.995, respectively. The root mean square errors (RMSEs) of the TMI and the AMSR-E SSTs with respect to the Argo observations are 0.74 and 0.73°C, respectively, which are higher than found by previous studies (e.g., Wentz et al., 2000; Senan et al., 2001; Bhaskar et al., 2009). These earlier studies used smaller ranges for validation; however, the moored buoy time series they used had more data points than the Argo NSTs used in our analysis.

3.3 *Temperature differences related to wind speed, water vapor, and cloud water*

The TMI/Argo and AMSR-E/Argo temperature differences were bin averaged for a range of physical parameters including not only satellite retrievals of wind speed and atmospheric water vapor (Dong et al., 2006), but also liquid cloud water. The largest temperature differences occur at low wind speed (Fig. 5). For example, on average, for wind speeds less than 5 m/s, both TMI and AMSR-E SSTs are warmer than the Argo NSTs, with maximum warming of about 0.5 and 1.5°C and mean values of 0.13 and 0.63°C, respectively (Table 1). Previous studies (Dong et al., 2006; Donlon et al., 2002; Gentemann et al., 2004) have found that the difference between skin and bulk temperatures have large variations at low wind speeds. Stronger winds tend to mix the water, causing small subskin-bulk SST differences. At low wind speeds, especially during daytime with solar insolation, subskin-bulk SST differences tend to be higher because of the effects of diurnal warming. For wind speeds greater than 5 m/s, the subskin-bulk SST differences become smaller, because wind-induced mixing homogenizes the upper few meters of the ocean. For wind speeds greater than 11 m/s, the standard deviation of the TMI/Argo temperature difference tends to increase (Fig. 5a) more rapidly than that of the AMSR-E/Argo. This implies that the AMSR-E SSTs might have smaller errors than the TMI SSTs under strong wind conditions. This strong wind effect is likely linked to a surface roughness, particularly to the formation of foam and spray, which in turn, leads to high sea surface emissivity. On average, for wind speeds greater than 15 m/s (here, wind speed measured using the 10.65 GHz channel), the TMI SSTs tend to be smaller than the Argo NSTs by about 0.36°C (Fig. 5, Table 1). This cool bias is more distinct with an average bias of –0.56°C if wind speeds are measured using the 37.0 GHz channel. However, the cool bias (about –0.08°C) is not distinct for the AMSR-E retrievals at high wind speeds. This result is consistent with the cool bias found by Gentemann and Wentz et al. (2001), and it implies that the TMI SSTs might be poorly calibrated under strong wind conditions.

Columnar water vapor is the second most important factor that affects the temperature differences, as has been found by some previous studies (Dong et al., 2006; Gille, 2012). Figure 6 shows that both TMI and AMSR-E SSTs are warmer on average than Argo NSTs when columnar water vapor is less than 8 mm, with mean warming of 0.80 and 0.64°C, respectively (Table 1). Radiation is affected by the absorption and emission of water vapor and cloud liquid water within the atmosphere and therefore, brightness temperatures measured by satellites differ from ground-based brightness temperature measurements (Brisson et al., 2002; Merchant and Le Borgne, 2004). Columnar water vapor is normally at its lowest in cold conditions; therefore, biases for low water vapor conditions are expected to have impact at high latitudes. This suggests there are calibration problems for the TMI and AMSR-E SSTs at high latitudes. Compared with low latitudes, there are fewer calibration data available for high latitudes, which might lead to poorer calibration under low water vapor conditions (Dong et al., 2006). The temperature differences become smaller when water vapor values are greater than 8 mm. By excluding data pairs for low water vapor conditions (< 8 mm), the average temperature differences between the TMI/AMSR-E SSTs and Argo NSTs are reduced from 0.05 and 0.20°C (Table 1) to –0.01 and 0.15°C, with mean standard deviations of 0.72 and 0.69°C, respectively. Therefore, the extensively distributed Argo NSTs could provide a data set with potential for eliminating the low water vapor effect in the TMI and AMSR-E SSTs.

Given the impact of columnar water vapor, liquid cloud water could also be suspected as a source of bias. However, the TMI/Argo and AMSR-E/Argo temperature differences hardly vary with liquid cloud water (Fig. 7). The mean standard devi-

Table 1. Mean temperature difference between satellite-retrieved SSTs and Argo NSTs, and the corresponding standard error against different parameters

Parameter	Wind speed/m·s^{-1}			Water vapor/mm		Cloud water/mm		
	0–22	<5	>15	0-60	<8	0–0.25	<0.06	>0.15
TMI–NST/°C	0.077±0.867	0.130±0.804	–0.364±1.124	0.053±0.753	0.796±1.270	–0.031±0.750	0.023±0.750	–0.051±0.832
AMSR-E–NST/°C	0.169±0.747	0.630±0.901	–0.084±0.780	0.203±0.695	0.635±0.748	–0.015±0.688	0.143±0.694	–0.187±0.788

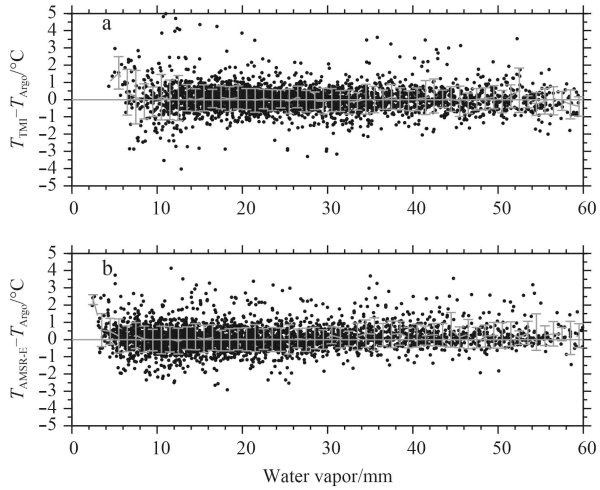

Fig. 6. Scatter plots of TMI (a) and AMSR-E SSTs (b) minus Argo NSTs versus water vapor measured by TMI and AMSR-E, respectively. Bin-averaged temperature differences based on latitude are marked as gray dashed lines. Error bars are twice the standard error for each bin.

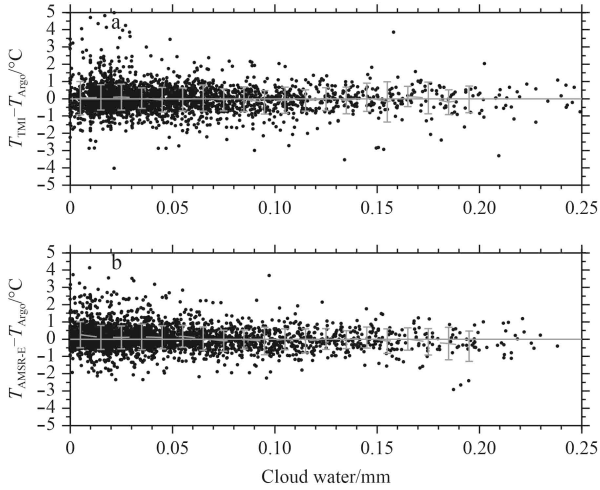

Fig. 7. Scatter plots of TMI (a) and AMSR-E SSTs (b) minus Argo NSTs versus cloud water measured by TMI and AMSR-E, respectively. Bin-averaged temperature differences based on latitude are marked as gray dashed lines. Error bars are twice the standard error for each bin.

ations of the temperature differences are 0.75 and 0.69°C for the TMI/Argo and the AMSR-E/Argo, respectively, with cloud water varying in a range of 0–0.2 mm. However, on average, the TMI SSTs tend to be warmer than the Argo NSTs by 0.2°C when liquid cloud water is low (< 0.06 mm). AMSR-E retrievals are colder than the Argo NSTs when liquid cloud water is high (> 0.15 mm) (Table 1), with a maximum value of about 0.4°C. This is consistent with the results from a comparison of the AMSR-E and global Argo 5 m temperatures (Gille, 2012).

3.4 *Latitudinal distribution*

Bin-averaged temperature differences based on latitude were calculated for both TMI/Argo and AMSR-E/Argo SSTs (Fig. 8). The standard deviations between the TMI/AMSR-E SSTs and the Argo NSTs are less than 1°C for most latitudes (with mean standard deviations of 0.56 and 0.54°C for the TMI/Argo and AMSR-E/Argo temperature differences, respectively), except for the mid-latitudes (35°–40°N) in the Northern Hemisphere for the TMI, and for 55°–60°S and 36°–52°N for the AMSR-E. The maximum standard deviation of the temperature differences can exceed 1.4 and 1.2°C between 35°N and 40°N for the TMI/Argo and the AMSR-E/Argo, respectively. Most Argo profiles between 35°N and 52°N are located near the Kuroshio, Oyashio, and Kuroshio Extension regions (Fig. 9), where the SST has distinct spatiotemporal variabilities (Miller et al., 1994; Deser and Blackmon, 1995; Qiu, 2000; Nonaka and Xie, 2003). Between 55°S and 60°S in the Southern Ocean, the presence of the Antarctic Circumpolar Current can lead to considerable variability of the SST (Hall and Visbeck, 2002; Verdy et al., 2006). Although there are few TMI/Argo and AMSR-E/Argo data pairs in the tropics (between 10°N and 15°N), their standard deviations of the temperature differences are smaller than in the mid- and high latitudes, with mean values of about 0.46 and 0.30°C, respectively.

3.5 *Comparison of TMI and AMSR-E SSTs with Argo NSTs in the Kuroshio and the Kuroshio Extension regions*

To compare the TMI and the AMSR-E SSTs with the Argo NSTs in the Kuroshio and Kuroshio Extension regions, we selected the Argo NSTs in two regions: 20°–30°N, 125°–135°E (Box B in Fig. 1) and 30°–40°N, 135°–168°E (Box A in Fig. 1). Both TMI and AMSR-E SSTs compare well with the *in situ* observations in these

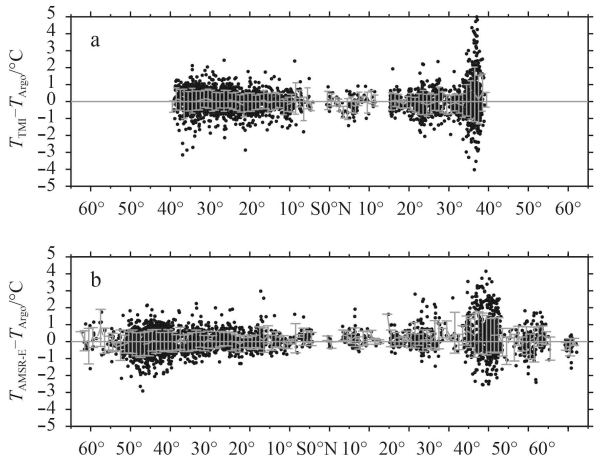

Fig. 8. Scatter plots of TMI (a) and AMSR-E SSTs (b) minus Argo NSTs versus latitude. Bin-averaged temperature differences based on latitude are marked as gray dashed lines. Error bars are twice the standard error for each bin.

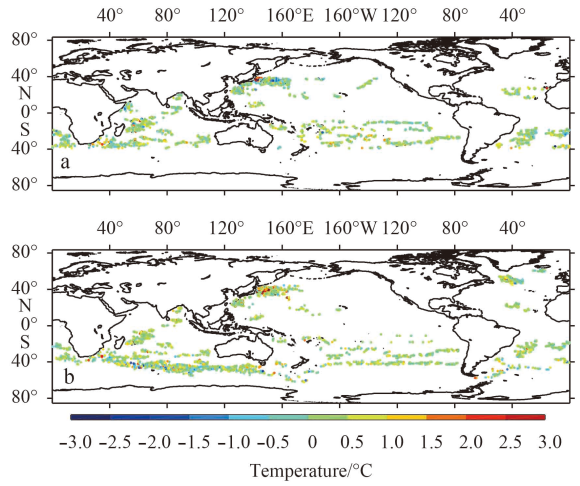

Fig. 9. Geographic distributions for TMI/Argo (a) and AMSR-E/Argo (b) data pairs. The colored dots indicate the temperature differences between the TMI/AMSR-E and the Argo at different locations.

regions. The correlation and the RMSE are slightly better for the AMSR-E SSTs than for the TMI SSTs (Table 2). The RMSEs for the TMI and AMSR-E SSTs with respect to the Argo NSTs in the region of the Kuroshio Extension are higher than in the Kuroshio region, with values of 1.27 and 1.21, respectively, i.e., the variability of the SST in the Kuroshio Extension region is greater than in the Kuroshio region. Some seasonal dependence of the temperature difference can still be seen in the Kuroshio Extension region (Fig. 10). The satellite-retrieved SSTs tend to be warmer than the *in situ* observations from February to August, with mean warming of 0.41 and 0.52°C for the TMI and the AMSR-E, respectively. However, on average, the satellite-retrieved SSTs are lower than the Argo NSTs in October and November. The maximum standard deviation of the temperature difference (up to 2.21°C) was observed in spring.

On average, the TMI and AMSR-E SSTs in the Kuroshio Extension region are warmer than the Argo NSTs when the wind speed is less than 8 m/s, with mean warming of 0.78 and 1.02°C, respectively (Fig. 11). A similar warming tendency by as much as 2.5°C is found in the Kuroshio region when the wind speed is less than 5 m/s (not shown). This implies that neither the TMI nor the AMSR-E SSTs in the regions of the Kuroshio and Kuroshio Extension are well calibrated at low wind speeds, and that the TMI might perform better than the AMSR-E. Similar to the results over the global oceans, the TMI and AMSR-E SSTs in the Kuroshio Extension region are slightly warmer than the Argo temperatures when columnar water vapor is less than 8 mm, with mean warming of 0.82 and 0.81°C, respectively (not shown); note, columnar water vapor of less than 8 mm was not observed in the Kuroshio region.

Table 2. Statistical results of comparison of the TMI and AMSR-E SSTs with the Argo NSTs in the Kuroshio and Kuroshio Extension (KE) regions

Region	Microwave sensor	Correlation coefficient	RMSE/°C	No. of data point
Box A (KE)	TMI	0.97	1.27	555
	AMSR-E	0.99	1.21	350
Box B (Kuroshio)	TMI	0.97	0.72	211
	AMSR-E	0.97	0.69	171

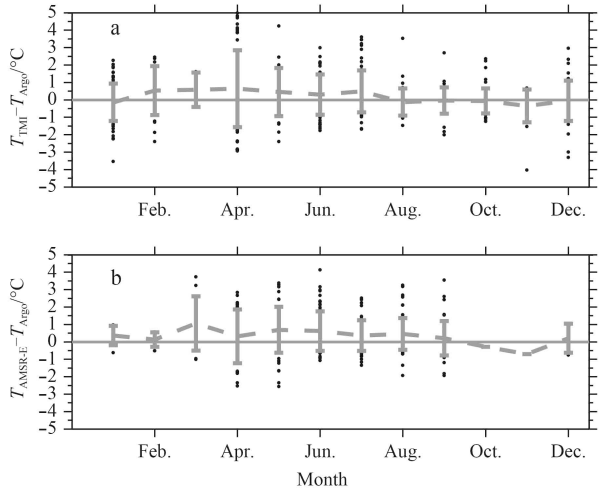

Fig. 10. Scatter plots of TMI (a) and AMSR-E SSTs (b) minus Argo NSTs versus month in Box A. Bin-averaged temperature differences based on month are marked as gray dashed lines. Error bars are twice the standard error for each bin.

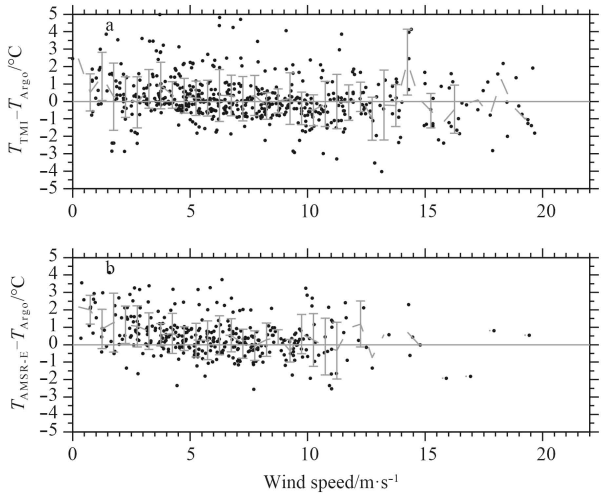

Fig. 11. Same as Fig. 5, except for the region of Box A in Fig. 1.

4 Conclusions

In this study, the Argo NSTs obtained within 1 m from the surface over the global oceans were used for comparison with the TMI/AMSR-E SSTs to analyze the relationships between the temperature differences and the satellite-retrieved wind speeds, atmospheric water vapor, liquid cloud water, and geographic location. Before the comparison, an analysis of the diurnal variability of the upper-ocean temperature was presented based on Argo near-surface and 5 m temperatures. Diurnal warming can be

found from 10:00 to 19:00 LT with maximum warming occurring at 14:00–15:00 LT. Diurnal cooling generally occurs before 08:00 LT. The seasonal dependence of this diurnal variability exists in both the Northern and Southern Hemispheres, with warming and cooling found in the summer and winter months, respectively, which probably results from increasing stratification in summer and seasonal changes in the upper-ocean stratification in winter. The comparison revealed high correlation between the satellite-retrieved SSTs and the Argo NSTs. When the wind speeds were less than 5 m/s, both TMI and AMSR-E SSTs have a warm bias relative to the Argo NSTs, which reflects the subskin-bulk temperature difference. The statistics of the comparison suggest that TMI performs slightly better than AMSR-E at low wind speeds, whereas the TMI SSTs might be poorly calibrated at high wind speeds.

The temperature differences under low water vapor (< 8 mm) show that both TMI and AMSR-E SSTs have a warm bias, which might reflect the sensitivity of the algorithm to low water vapor conditions. Such a situation often occurs at high latitudes where the numbers of the *in situ* data collected and available for validation of satellite-retrieved SSTs are few.

The analysis of the spatial distribution show that both TMI and AMSR-E SSTs are in good agreement with the Argo NSTs at low latitudes. The maximum variations of the temperature difference were found near the Kuroshio, Oyashio, and Kuroshio Extension regions in the northern Pacific, as well as at 55°–60°S in the southern Ocean. Further analysis of the region of the Kuroshio and its extension shows that the variability of the SST in the Kuroshio Extension is higher than in the Kuroshio region. A seasonal dependence of the temperature difference was found in the Kuroshio Extension, which revealed lower variability of the temperature difference in spring. Both TMI and AMSR-E SSTs in the region of the Kuroshio and its extension are poorly calibrated at low wind speeds (< 8 m/s), although the TMI might perform better than the AMSR-E in these regions.

As the Argo real-time ocean observing array is expected to be maintained for at least a further 10 a, it will provide time series profiles over the global oceans that are more accurate than from TAO buoys, which could produce a data set with potential for the validation of satellite-retrieved data. In comparison with other *in situ* observations, the Argo NSTs might be more suitable for validation and evaluation of satellite-retrieved SSTs because of their higher accuracy and greater coverage.

Acknowledgements

The Argo near-surface temperature data were collected and made freely available by the National Oceanography Centre (NOC). The TMI and AMSR-E data are produced by remote sensing systems and sponsored by the NASA Earth Science REASON DISCOVER Project and the AMSR-E Science Team. Data are available at www.remss.com.

References

Barton I J. 1995. Satellite-derived sea surface temperatures: current status. Journal of Geophysical Research, 100(C5): 8777–8790

Bhaskar T V S U, Rahman S H, Pavan I D, et al. 2009. Comparison of AMSR-E and TMI sea surface temperature with Argo near-surface temperature over the Indian Ocean. International Journal of Remote Sensing, 30(10): 2669–2684

Bhat G S, Vecchi G A, Gadgil S. 2004. Sea surface temperature of the Bay of Bengal derived from the TRMM microwave imager. Journal of Atmospheric and Oceanic Technology, 21(8): 1283–1290

Brisson A, Le Borgne P, Marsouin A. 2002. Results of one year of preoperational production of sea surface temperatures from GOES-8. Journal of Atmospheric and Oceanic Technology, 19(10): 1638–1652

Brown O B, Brown J W, Evans R H. 1985. Calibration of advanced very high resolution radiometer infrared observations. Journal of Geophysical Research, 90(C6): 11667–11677

Curry J A, Bentamy A, Bourassa M A, et al. 2004. Seaflux. Bulletin of the American Meteorological Society, 85(3): 409–424

Deser C, Blackmon M L. 1995. On the relationship between tropical and North Pacific sea surface temperature variations. Journal of Climate, 8(6): 1677–1680

Dong S, Gille S T, Sprintall J, et al. 2006. Validation of the advanced microwave scanning radiometer for the earth observing system (AMSR-E) sea surface temperature in the Southern Ocean. Journal of Geophysical Research, 111(C4): C04002

Donlon C J, Minnett P J, Gentemann C, et al. 2002. Toward improved validation of satellite sea surface skin temperature measurements for climate research. Journal of Climate, 15(4): 353–369

Donlon C J, Robinson I, Casey K S, et al. 2007. The global ocean data assimilation experiment high—resolution sea surface temperature pilot project. Bulletin of the American Meteorological Society, 88(8): 1197–1213

Emery W J, Yu Y, Wick G A, et al. 1994. Correcting infrared satellite estimates of sea surface temperature for atmospheric water vapor attenuation. Journal of Geophysical Research, 99(C3): 5219–5236

Flament P, Firing J, Sawyer M, et al. 1994. Amplitude and horizontal structure of a large diurnal sea-surface warming event during the coastal ocean dynamics experiment. Journal of Physical Oceanography, 24(1): 124–139

Gentemann C L, Wentz F J. 2001. Satellite microwave SST: accuracy, comparisons to AVHRR and Reynolds SST, and measurement of diurnal thermocline variability. Geoscience and Remote Sensing Symposium, 2001. IGARSS '01. IEEE 2001 International. IEEE, 1: 246–248

Gentemann C L, Donlon C J, Stuart-Menteth A, et al. 2003. Diurnal signals in satellite sea surface temperature measurements. Geophysical Research Letters, 30(3): 1140

Gentemann C L, Wentz F J, Mears C A, et al. 2004. In situ validation of tropical rainfall measuring mission microwave sea surface temperatures. Journal of Geophysical Research, 109(C4): C04021

Gentemann C L, Minnett P J. 2008. Radiometric measurements of ocean surface thermal variability. Journal of Geophysical Research, 113(C8): C08017

Gentemann C L, Minnett P J, Le Borgne P, et al. 2008. Multi-satellite measurements of large diurnal warming events. Geophysical Research Letters, 35(22): L22602

Gille S T. 2012. Diurnal variability of upper ocean temperatures from microwave satellite measurements and Argo profiles. Journal of Geophysical Research: Oceans, 117(C11): C11027

Guan L, Kawamura H. 2003. SST availabilities of satellite infrared and microwave measurements. Journal of Oceanography, 59(2): 201–209

Hall A, Visbeck M. 2002. Synchronous variability in the southern hemisphere atmosphere, sea ice, and ocean resulting from the annular mode. Journal of Climate, 15(21): 3043–3057

McClain E P. 1989. Global sea surface temperatures and cloud clearing for aerosol optical depth estimates. International Journal of Remote Sensing, 10(4–5): 763–769

McPhaden M J. 1999. Genesis and evolution of the 1997–98 El Niño. Science, 283(5404): 950–954

Merchant C J, Le Borgne P. 2004. Retrieval of sea surface temperature from space, based on modeling of infrared radiative transfer: capabilities and limitations. Journal of Atmospheric and Oceanic Technology, 21(11): 1734–1746

Merchant C J, Filipiak M J, Le Borgne P, et al. 2008. Diurnal warm-layer events in the western Mediterranean and European shelf seas. Geophysical Research Letters, 35(4): L04601

Miller A J, Cayan D R, Barnett T P, et al. 1994. Interdecadal variability of the Pacific Ocean: model response to observed heat flux and wind stress anomalies. Climate Dynamics, 9(6): 287–302

Muraleedharan P M, Pankajakshan T, Harikrishnan M. 2004. Validation of multi-channel scanning microwave radiometer onboard Oceansat—I. Current Science, 87(3): 370–376

Nonaka M, Xie S. 2003. Covariations of sea surface temperature and wind over the Kuroshio and its extension: evidence for ocean-to-atmosphere feedback. Journal of Climate, 16(9): 1404–1413

Pandey P C, Kniffen S. 1991. Linear retrieval, validation and mapping of the sea surface temperature over western mid-latitude North Pacific using Seasat SMMR data. International Journal of Remote Sensing, 12(12): 2493–2511

Parekh A, Sharma R, Sarkar A. 2007. A comparative assessment of surface wind speed and sea surface temperature over the Indian Ocean by TMI, MSMR, and ERA-40. Journal of Atmospheric and Oceanic Technology, 24(6): 1131–1142

Qiu Bo. 2000. Interannual variability of the Kuroshio extension system and its impact on the wintertime SST field. Journal of Physical Oceanography, 30(6): 1486–1502

Senan R, Anith D S, Sengupta D. 2001. Validation of SST and windspeed from TRMM using North Indian Ocean moored buoy observations. CAOS Report 2001 AS1. Bangalore: Indian Institute of Science and Technology

Suarez M J, Schopf P S. 1988. A delayed action oscillator for ENSO. Journal of the Atmospheric Sciences, 45(21): 3283–3287

Verdy A, Marshall J, Czaja A. 2006. Sea surface temperature variability along the path of the Antarctic Circumpolar Current. Journal of Physical Oceanography, 36(7): 1317–1331

Wentz F J. 1998. Algorithm theoretical basis document: AMSR ocean algorithm. Technical Report 050198. California: Remote Sensing Systems

Wentz F J, Meissner T. 1999. AMSR Ocean Algorithm (Version 2). Technical Report 121599a. California: Remote Sensing Systems

Wentz F J, Gentemann C L, Smith D K, et al. 2000. Satellite measurements of sea surface temperature through clouds. Science, 288(5467): 847–850

Wentz F J, Ashcroft P D, Gentemann C L. 2001. Post-launch calibration of the TRMM microwave imager. IEEE Transactions on Geoscience and Remote Sensing, 39(2): 415–422

Wentz F J, Gentemann J C, Ashcroft P. 2003. On-orbit calibration of AMSR-E and the retrieval of ocean products. California: Remote Sensing Systems